

Onboard LiDAR-based Detection

M. Švehlík¹, V. Váňa², M. Pěšák³, M. B. P. Trnka⁴, V. P. Špalek⁵,
D. Heřmánek¹, J. M. Škarda¹, M. Š. P. Trnka¹

Abstract—A new robust and accurate approach for the detection and localization of flying objects with the purpose of highly dynamic aerial interception and agile multi-robot interaction is presented in this paper. The approach is proposed for use onboard an autonomous aerial vehicle equipped with a 3D Light Detection and Ranging (LiDAR) sensor providing input data for the algorithm. It relies on a novel 3D occupancy voxel mapping method for the target detection and a cluster-based multiple hypothesis tracker to compensate uncertainty of the sensory data. When compared to state-of-the-art methods of onboard detection of other flying objects, the presented approach provides superior localization accuracy and robustness to different environments and appearance changes of the target, as well as a greater detection range. Furthermore, in combination with the proposed multi-target tracker, sporadic false positives are suppressed, state estimation of the target is provided and the detection latency is negligible. This makes the detector suitable for tasks of agile multi-robot interaction, such as autonomous aerial interception or formation control where precise, robust, and fast relative localization of other robots is crucial. We demonstrate the practical usability and performance of the system in simulated and real-world experiments.

I. INTRODUCTION

What is this paper about? This paper presents a new robust and accurate approach for the detection and localization of flying objects with the purpose of highly dynamic aerial interception and agile multi-robot interaction. The approach is proposed for use onboard an autonomous aerial vehicle equipped with a 3D Light Detection and Ranging (LiDAR) sensor providing input data for the algorithm. It relies on a novel 3D occupancy voxel mapping method for the target detection and a cluster-based multiple hypothesis tracker to compensate uncertainty of the sensory data. When compared to state-of-the-art methods of onboard detection of other flying objects, the presented approach provides superior localization accuracy and robustness to different environments and appearance changes of the target, as well as a greater detection range. Furthermore, in combination with the proposed multi-target tracker, sporadic false positives are suppressed, state estimation of the target is provided and the detection latency is negligible. This makes the detector suitable for tasks of agile multi-robot interaction, such as autonomous aerial interception or formation control where precise, robust, and fast relative localization of other robots is crucial. We demonstrate the practical usability and performance of the system in simulated and real-world experiments.



Fig. 1: The proposed system architecture.

How is this paper structured? The paper is structured as follows. Section II describes the system architecture. Section III describes the proposed approach for the detection and localization of flying objects. Section IV describes the proposed multi-target tracker. Section V describes the experimental setup and results. Section VI concludes the paper.

¹ This work is supported by the Czech Science Foundation (GAJ19/0015S).

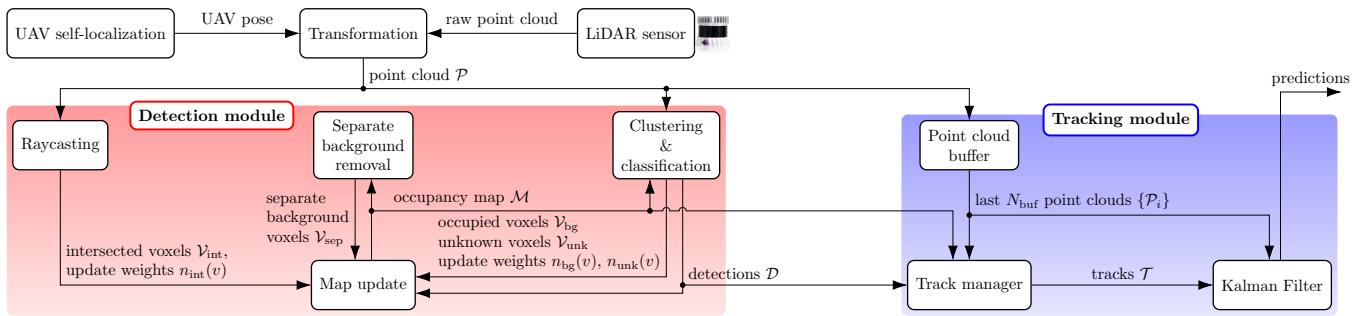


Fig. 2: Overview of the proposed system architecture.

This paper presents a novel system for 3D object tracking on a UAV. It is designed to be robust to clutter and dynamic environments. The system consists of a detection module and a tracking module. The detection module uses raycasting to identify potential objects and an occupancy map to manage background clutter. The tracking module uses a point cloud buffer and a Kalman filter to maintain and predict object positions.

2 (in Fig 1)

This paper presents a novel system for 3D object tracking on a UAV. It is designed to be robust to clutter and dynamic environments. The system consists of a detection module and a tracking module. The detection module uses raycasting to identify potential objects and an occupancy map to manage background clutter. The tracking module uses a point cloud buffer and a Kalman filter to maintain and predict object positions.

This paper presents a novel system for 3D object tracking on a UAV. It is designed to be robust to clutter and dynamic environments. The system consists of a detection module and a tracking module. The detection module uses raycasting to identify potential objects and an occupancy map to manage background clutter. The tracking module uses a point cloud buffer and a Kalman filter to maintain and predict object positions.

This paper presents a novel system for 3D object tracking on a UAV. It is designed to be robust to clutter and dynamic environments. The system consists of a detection module and a tracking module. The detection module uses raycasting to identify potential objects and an occupancy map to manage background clutter. The tracking module uses a point cloud buffer and a Kalman filter to maintain and predict object positions.

This paper presents a novel system for 3D object tracking on a UAV. It is designed to be robust to clutter and dynamic environments. The system consists of a detection module and a tracking module. The detection module uses raycasting to identify potential objects and an occupancy map to manage background clutter. The tracking module uses a point cloud buffer and a Kalman filter to maintain and predict object positions.

$$O(1) \text{ per}$$

$$O(n^2) \text{ per}$$

A. Related works

This paper presents a novel system for 3D object tracking on a UAV. It is designed to be robust to clutter and dynamic environments. The system consists of a detection module and a tracking module. The detection module uses raycasting to identify potential objects and an occupancy map to manage background clutter. The tracking module uses a point cloud buffer and a Kalman filter to maintain and predict object positions.

This paper presents a novel system for 3D object tracking on a UAV. It is designed to be robust to clutter and dynamic environments. The system consists of a detection module and a tracking module. The detection module uses raycasting to identify potential objects and an occupancy map to manage background clutter. The tracking module uses a point cloud buffer and a Kalman filter to maintain and predict object positions.

LDAR in

II. NOTATION

M is the environment map, \mathcal{V} is the set of vertices, \mathcal{P} is the set of polygons, S is the set of sensor rays, $v(p)$ is the probability of a vertex v being occupied by a polygon p , $\|c_{v_1} - c_{v_2}\|$ and $\|c_v - p\|$ are the distances between vertices v_1 and v_2 , and between vertex v and polygon p , respectively.

III. FLING OBJECTS DETECTION ALGORITHM

The algorithm is shown in Fig. 2. It consists of a Detection module and a Tracking module. The Detection module takes the LDAR data and the UAV's position as input and outputs the set of polygons \mathcal{P} and the set of vertices \mathcal{V}_b (background polygons) and \mathcal{V}_h (tentative occupied polygons). The Tracking module takes the set of polygons \mathcal{P} and the set of vertices \mathcal{V}_h as input and outputs the set of polygons \mathcal{D} (confident free polygons) and the set of vertices \mathcal{N}_b (confident occupied polygons). The algorithm uses a Kalman Filter (KF) for tracking.

The algorithm is implemented in MATLAB and C++ using ROS in a MRS UAV system. The system uses 6 CPUs and 3 GPUs.

3. D

A. Environment occupancy mapping and representation

The environment occupancy mapping is represented by the probability $p(v | z_{[1:t]})$ of a vertex v being occupied by a polygon p given the sensor data $z_{[1:t]}$.

$$L(v | z_{[1:t]}) = \log \left(\frac{p_o(v | z_{[1:t]})}{1 - p_o(v | z_{[1:t]})} \right), \quad (1)$$

where $p_o(v | z_{[1:t]})$ is the probability of a vertex v being occupied by a polygon p given the sensor data $z_{[1:t]}$.

$$p(A | B) = \frac{p(B | A)p(A)}{p(B)}. \quad (2)$$

Eq. (2) is used to calculate the probability of a vertex v being occupied by a polygon p given the sensor data $z_{[1:t]}$.

The algorithm uses a Bayesian approach to calculate the probability of a vertex v being occupied by a polygon p given the sensor data $z_{[1:t]}$.

$$L(v | z_{[1:t]}) = L(v | z_{[1:t-1]}) + L(v | z_{[t]}) \quad (3)$$

where $L(v | z_{[1:t-1]})$ and $L(v | z_{[t]})$ are the probabilities of a vertex v being occupied by a polygon p given the sensor data $z_{[1:t-1]}$ and $z_{[t]}$, respectively.

The algorithm uses a Bayesian approach to calculate the probability of a vertex v being occupied by a polygon p given the sensor data $z_{[1:t]}$.

$$L(v) = \begin{cases} L_o & \text{if } L(v) \geq L_o, \\ L_\epsilon & \text{if } L(v) \leq L_\epsilon, \\ 0 & \text{otherwise.} \end{cases} \quad (4)$$

The algorithm uses a Bayesian approach to calculate the probability of a vertex v being occupied by a polygon p given the sensor data $z_{[1:t]}$.

probabilistic

[5] [6] [7] [8]

probabilistic

probabilistic

probabilistic

probabilistic

probabilistic

probabilistic

probabilistic

probabilistic

probabilistic

probabilistic

probabilistic

probabilistic

probabilistic

probabilistic

probabilistic

probabilistic

probabilistic

probabilistic

probabilistic

probabilistic

probabilistic

probabilistic

probabilistic

probabilistic

probabilistic

probabilistic

probabilistic

probabilistic

probabilistic

probabilistic

probabilistic

probabilistic

probabilistic

probabilistic

probabilistic

probabilistic

probabilistic

probabilistic

probabilistic

probabilistic

probabilistic

probabilistic

probabilistic

probabilistic

probabilistic

probabilistic

probabilistic

probabilistic

probabilistic

probabilistic

probabilistic

probabilistic

probabilistic

probabilistic

probabilistic

probabilistic

probabilistic

probabilistic

probabilistic

probabilistic

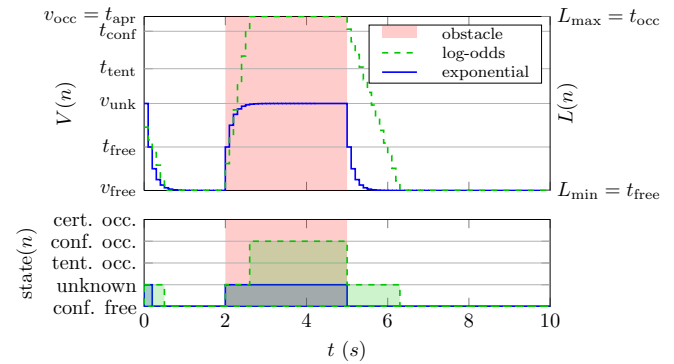


Fig. 3: Clustering & classification

at $t = 4.5$ s.

at $t = 2$ s.

at $t = 4.5$ s.

at $t = 2$ s.

at $t = 4.5$ s.

at $t = 2$ s.

at $t = 4.5$ s.

at $t = 2$ s.

at $t = 4.5$ s.

at $t = 2$ s.

at $t = 4.5$ s.

at $t = 2$ s.

at $t = 4.5$ s.

at $t = 2$ s.

at $t = 4.5$ s.

at $t = 2$ s.

at $t = 4.5$ s.

at $t = 2$ s.

at $t = 4.5$ s.

at $t = 2$ s.

at $t = 4.5$ s.

at $t = 2$ s.

at $t = 4.5$ s.

at $t = 2$ s.

at $t = 4.5$ s.

at $t = 2$ s.

at $t = 4.5$ s.

at $t = 2$ s.

at $t = 4.5$ s.

at $t = 2$ s.

at $t = 4.5$ s.

at $t = 2$ s.

at $t = 4.5$ s.

at $t = 2$ s.

at $t = 4.5$ s.

at $t = 2$ s.

at $t = 4.5$ s.

at $t = 2$ s.

at $t = 4.5$ s.

at $t = 2$ s.

at $t = 4.5$ s.

at $t = 2$ s.

at $t = 4.5$ s.

at $t = 2$ s.

at $t = 4.5$ s.

at $t = 2$ s.

at $t = 4.5$ s.

at $t = 2$ s.

at $t = 4.5$ s.

$L(v)$ and $G(v)$ at $t = 2$ s.

$L(v)$ and $G(v)$ at $t = 4.5$ s.

$L(v)$ and $G(v)$ at $t = 2$ s.

$L(v)$ and $G(v)$ at $t = 4.5$ s.

$L(v)$ and $G(v)$ at $t = 2$ s.

$L(v)$ and $G(v)$ at $t = 4.5$ s.

$L(v)$ and $G(v)$ at $t = 2$ s.

$L(v)$ and $G(v)$ at $t = 4.5$ s.

$L(v)$ and $G(v)$ at $t = 2$ s.

$L(v)$ and $G(v)$ at $t = 4.5$ s.

$L(v)$ and $G(v)$ at $t = 2$ s.

$L(v)$ and $G(v)$ at $t = 4.5$ s.

$L(v)$ and $G(v)$ at $t = 2$ s.

$L(v)$ and $G(v)$ at $t = 4.5$ s.

$L(v)$ and $G(v)$ at $t = 2$ s.

$L(v)$ and $G(v)$ at $t = 4.5$ s.

$L(v)$ and $G(v)$ at $t = 2$ s.

$L(v)$ and $G(v)$ at $t = 4.5$ s.

$L(v)$ and $G(v)$ at $t = 2$ s.

$L(v)$ and $G(v)$ at $t = 4.5$ s.

$L(v)$ and $G(v)$ at $t = 2$ s.

$L(v)$ and $G(v)$ at $t = 4.5$ s.

$L(v)$ and $G(v)$ at $t = 2$ s.

$L(v)$ and $G(v)$ at $t = 4.5$ s.

$L(v)$ and $G(v)$ at $t = 2$ s.

$L(v)$ and $G(v)$ at $t = 4.5$ s.

$L(v)$ and $G(v)$ at $t = 2$ s.

$L(v)$ and $G(v)$ at $t = 4.5$ s.

$L(v)$ and $G(v)$ at $t = 2$ s.

$L(v)$ and $G(v)$ at $t = 4.5$ s.

$L(v)$ and $G(v)$ at $t = 2$ s.

$$G(v) = \begin{cases} f & \text{if } G(v) \geq G_{N_n}, \\ i, & \text{if } G(v) \in [G_i, G_{i+1}), \\ f & \text{if } G(v) < G_1. \end{cases} \quad (6)$$

$$G(v) = \begin{cases} f & \text{if } G(v) \geq G_n, \\ f & \text{if } G(v) \in [G_n, G_n), \\ f & \text{if } G(v) \in [G_n, G_n), \\ f & \text{if } G(v) < G_n. \end{cases} \quad (7)$$

$$G(v | z_{[1:t]}) = \frac{G(v | z_{[1:t-1]}) + G(v | z_{[t]})}{2}, \quad (8)$$

$$G(v | z_{[t]}) = g_i, \quad i = 1, 2, \dots, N_n, \quad (9)$$

$$G(v | z_{[t]}) = \begin{cases} g_o & \text{if } v \in \mathcal{V}_o, \\ g_h & \text{if } v \in \mathcal{V}_h \cup \mathcal{V}_d, \\ g_e & \text{if } v \in \mathcal{V}_h, \end{cases} \quad (9)$$

$\mathcal{V}_o, \mathcal{V}_h, \mathcal{V}_d, \mathcal{V}_h$ are defined in Fig. 2.

If $v \in \mathcal{V}_o$, then $G(v) = g_o$.

If $v \in \mathcal{V}_h \cup \mathcal{V}_d$, then $G(v) = g_h$.

If $v \in \mathcal{V}_h$, then $G(v) = g_e$.

If $v \in \mathcal{V}_o$, then $G(v) = g_o$.

If $v \in \mathcal{V}_h \cup \mathcal{V}_d$, then $G(v) = g_h$.

If $v \in \mathcal{V}_h$, then $G(v) = g_e$.

If $v \in \mathcal{V}_o$, then $G(v) = g_o$.

$L(v)$ and $G(v)$ at $t = 2$ s.

$L(v)$ and $G(v)$ at $t = 4.5$ s.

$L(v)$ and $G(v)$ at $t = 2$ s.

$L(v)$ and $G(v)$ at $t = 4.5$ s.

$L(v)$ and $G(v)$ at $t = 2$ s.

$L(v)$ and $G(v)$ at $t = 4.5$ s.

$L(v)$ and $G(v)$ at $t = 2$ s.

$L(v)$ and $G(v)$ at $t = 4.5$ s.

$L(v)$ and $G(v)$ at $t = 2$ s.

$L(v)$ and $G(v)$ at $t = 4.5$ s.

$L(v)$ and $G(v)$ at $t = 2$ s.

$L(v)$ and $G(v)$ at $t = 4.5$ s.

$L(v)$ and $G(v)$ at $t = 2$ s.

$L(v)$ and $G(v)$ at $t = 4.5$ s.

$L(v)$ and $G(v)$ at $t = 2$ s.

$L(v)$ and $G(v)$ at $t = 4.5$ s.

$L(v)$ and $G(v)$ at $t = 2$ s.

$L(v)$ and $G(v)$ at $t = 4.5$ s.

$L(v)$ and $G(v)$ at $t = 2$ s.

$L(v)$ and $G(v)$ at $t = 4.5$ s.

$L(v)$ and $G(v)$ at $t = 2$ s.

$L(v)$ and $G(v)$ at $t = 4.5$ s.

$L(v)$ and $G(v)$ at $t = 2$ s.

$L(v)$ and $G(v)$ at $t = 4.5$ s.

$L(v)$ and $G(v)$ at $t = 2$ s.

$L(v)$ and $G(v)$ at $t = 4.5$ s.

$L(v)$ and $G(v)$ at $t = 2$ s.

$L(v)$ and $G(v)$ at $t = 4.5$ s.

$L(v)$ and $G(v)$ at $t = 2$ s.

$L(v)$ and $G(v)$ at $t = 4.5$ s.

$L(v)$ and $G(v)$ at $t = 2$ s.

B. Clustering & classification

The flying object, v , is classified into one of the clusters $\mathcal{V}_o, \mathcal{V}_h, \mathcal{V}_d, \mathcal{V}_h$.

The probability of being in each cluster is $P(v \in \mathcal{V}_o) = p_o, P(v \in \mathcal{V}_h) = p_h, P(v \in \mathcal{V}_d) = p_d, P(v \in \mathcal{V}_h) = p_h$.

The probability of being in each cluster is $P(v \in \mathcal{V}_o) = p_o, P(v \in \mathcal{V}_h) = p_h, P(v \in \mathcal{V}_d) = p_d, P(v \in \mathcal{V}_h) = p_h$.

The probability of being in each cluster is $P(v \in \mathcal{V}_o) = p_o, P(v \in \mathcal{V}_h) = p_h, P(v \in \mathcal{V}_d) = p_d, P(v \in \mathcal{V}_h) = p_h$.

Algorithm 1

$C_k, C_l, k \neq l,$

$$C_k \cap C_l = \emptyset, \quad (13)$$

$$\forall \{p_i \in C_k, p_j \in C_l\}, \|p_i - p_j\| > d_b, \quad (14)$$

Algorithm 2

$p_i, p_j \in C_k,$

$\{p_c, p_{c+1}, \dots, p_{c+n}\} \subset C_k$

$$\|p_i - p_c\| \leq d_b, \quad (15)$$

$$\|p_c - p_{c+1}\| \leq d_b, \quad (15)$$

$\dots,$

$$\|p_{c+n} - p_j\| \leq d_b.$$

Algorithm 3

C

A) If \dots

d_b *tentative occupied,*

background.

B) If A) \dots

confident free \dots *tentative occupied* \dots *flying object.*

C) If \dots A) \dots B) \dots a unknown.

From p, \dots A) \dots

\dots

$$l = 2d_b + 1, \dots$$

$$\|c_v - p\| < d_b$$

$G(v) \geq G_b$ \dots

\dots

\dots

$O(nl^2).$

This B) is \dots . The

BFS (BFS) \dots

\dots

tentative occupied \dots *confident*

free \dots $v(p), p \in C, \dots$

\dots

B) \dots

C (15-17) \dots

\dots

uncertain \dots

\dots

\dots

\dots

\dots

tentative occupied \dots

$v(p), p \in C, \dots$

confident free \dots B) \dots

\dots

Let \mathcal{P}_b \dots

background, \mathcal{P}_d \dots

objects, \mathcal{P}_k \dots *unknown* \dots

$\mathcal{P}_d = \mathcal{P}_b \cap \mathcal{P}_k = \mathcal{P}_d \cap \mathcal{P}_k = \emptyset.$ The

\dots

$$\mathcal{V}_b = \{v(p) \mid p \in \mathcal{P}_b\}, \quad n_b(v) = |\mathcal{P}_b \cap v|, \quad (16)$$

$$\mathcal{V}_d = \{v(p) \mid p \in \mathcal{P}_d\}, \quad n_d(v) = \infty, \quad (17)$$

$$\mathcal{V}_k = \{v(p) \mid p \in \mathcal{P}_k\}, \quad n_k(v) = |\mathcal{P}_k \cap v|. \quad (18)$$

Then n_k \dots

\dots

C_D \dots

r_D \dots

Algorithm 1 BFS

1: **Input:**

2: $C = \{p_1, p_2 \dots p_N\}$

3: \mathcal{M}

4: **Output:**

5: $\text{floating} \in \{b, k\}$

6: **Parameters:**

7: $d_b \in \mathbb{N}$

8: **for** $p \in C$ **do**

9: $v_0 := v(p)$

10: $\mathcal{V}_b := \emptyset$

11: $\mathcal{V}_q := \{v_0\}$

12: **while** $\mathcal{V}_q \neq \emptyset$ **do**

13: $v := p(\mathcal{V}_q)$

14: $\text{tentative occupied}$

15: **if** $G(v) \geq G_b$ **then**

16: $\text{return flg} := k$

17: **end if**

18: uncertain, k

19: **if** $G(v) \in [G_a, G_b)$ **then**

20: $\text{tentative occupied}$

21: **if** $\|c_v - c_{v_0}\|_1 \geq d_b$ **then**

22: $\text{return flg} := k$

23: **end if**

24: $\text{tentative occupied}$

25: **for** $v_b \in \mathcal{V}_q$ **do**

26: **if** $v_b \notin \mathcal{V}_b \wedge v_b \in \mathcal{M}$ **then**

27: $\mathcal{V}_q(v_b, \mathcal{V}_q)$

28: **end if**

29: **end for**

30: **end if**

31: confident free

32: $\mathcal{V}_b := \mathcal{V}_b \cup v$

33: **end while**

34: **end for**

35: $\text{return flg} := b$

D \dots

$$r_D = \frac{1}{|C_D|} \sum_{p \in C_D} p = c(C_D), \quad (19)$$

$c(C_D)$ \dots

$C_D.$

C. Raycasting

A \dots

\dots \mathcal{V}_b

\dots $n_b(v).$

\dots \mathcal{P} is *organized point cloud*,

\dots $p \in \mathcal{P}$ \dots \mathcal{P}

\dots \mathcal{P}

\dots \mathcal{P}

\dots \mathcal{P}

\dots \mathcal{P}

\dots \mathcal{P}

\dots \mathcal{P}

\dots \mathcal{P}

\dots \mathcal{P}

\dots \mathcal{P}

\dots \mathcal{P}

\dots \mathcal{P}

\dots \mathcal{P}

\dots \mathcal{P}

\dots \mathcal{P}

\dots \mathcal{P}

\dots \mathcal{P}

\mathcal{P} contains $p_i \in \mathcal{P}$ with r_i and c_a are the center of mass of the point cloud \mathcal{P} . e_i is the vector from c_a to p_i . d_m is the maximum distance from c_a to any point in \mathcal{P} . \vec{d}_i is the normalized vector from c_a to p_i .

$$e_i = \begin{cases} c_a + d_m \vec{d}_i, & \text{if } p_i = p_m, \\ c_a + \min(d_m, \|p_i - c_a\|) \vec{d}_i, & \text{else} \end{cases} \quad (20)$$

\mathcal{R} is the set of all possible ranges $r \in \mathcal{R}$. $l_h(v, r)$ is the number of points in \mathcal{V}_h at range r from voxel v . $n_h(v)$ is the total number of points in \mathcal{V}_h around voxel v .

$$\mathcal{V}_h = \{v \mid \exists r \in \mathcal{R}, l_h(v, r) \neq 0\}, \quad (21)$$

$$n_h(v) = \sum_{r \in \mathcal{R}} l_h(v, r). \quad (22)$$

D. Separate background voxel removal

The initial map \mathcal{M} is a set of tentative occupied voxels. \mathcal{M} is updated by the LiDAR sensor. \mathcal{M} is divided into confident occupied voxels \mathcal{V}_p and tentative occupied voxels \mathcal{V}_t . \mathcal{V}_p is the set of voxels that have been observed by the LiDAR sensor for a long time. \mathcal{V}_t is the set of voxels that have been observed by the LiDAR sensor for a short time. \mathcal{V}_p and \mathcal{V}_t are defined as follows:

$$\mathcal{V}_p = \{v \in \mathcal{V}_h \mid G(v) \geq G_p\} \quad \text{and} \quad \mathcal{V}_t = \{v \in \mathcal{V}_h \mid G(v) < G_p\}. \quad (23)$$

$G(v)$ is the number of points in \mathcal{V}_h around voxel v . G_p is the threshold for the number of points in \mathcal{V}_h around voxel v . $n_p(v)$ is the number of points in \mathcal{V}_p around voxel v .

E. A priori map initialization

The initial map \mathcal{M} is initialized with a set of unknown voxels \mathcal{V}_u . \mathcal{V}_u is the set of voxels that have not been observed by the LiDAR sensor. \mathcal{V}_u is defined as follows:

\mathcal{P} contains $p_i \in \mathcal{P}$ with r_i and c_a are the center of mass of the point cloud \mathcal{P} . e_i is the vector from c_a to p_i . d_m is the maximum distance from c_a to any point in \mathcal{P} . \vec{d}_i is the normalized vector from c_a to p_i .

F. LiDAR-based multi-target tracking

The LiDAR-based multi-target tracking algorithm is described in Algorithm 2. The algorithm maintains a set of tracks \mathcal{T} and a set of points \mathcal{P} . The algorithm updates the tracks and points at each time step t . The algorithm uses a Kalman filter (KF) to track the targets. The algorithm uses a LiDAR sensor to observe the targets. The algorithm uses a LiDAR sensor to observe the targets. The algorithm uses a LiDAR sensor to observe the targets.

1) Track update: The updateTrack() function (Fig. 2) updates the tracks \mathcal{T} and the points \mathcal{P} . The updateTrack() function uses the LiDAR sensor to observe the targets. The updateTrack() function uses the Kalman filter to track the targets. The updateTrack() function uses the LiDAR sensor to observe the targets.

$$\hat{x}_T = \begin{bmatrix} \hat{r}_T^T & \hat{v}_T^T & \hat{a}_T^T \end{bmatrix}^T \quad (24)$$

$$x = \begin{bmatrix} r^T & \vec{v}^T & \vec{a}^T \end{bmatrix}^T, \quad (25)$$

$r \in \mathbb{R}^3$ is the range, $\vec{v} \in \mathbb{R}^3$ is the velocity, and $\vec{a} \in \mathbb{R}^3$ is the acceleration. P_T is the covariance matrix of the target state. $n_d(T)$ is the number of detections for track T . $\Delta t_{[k]} = t_{[k]} - t_{[k-1]}$ is the time interval between the current time step $t_{[k]}$ and the previous time step $t_{[k-1]}$. r_0 is the initial range. $r_0 : \mathbb{R}^{3 \times 3} \rightarrow \mathbb{R}$ is the initial range matrix. $r_0(P_T) = \max(r_m, c_r \sqrt{|HP_T H^T|})$, where r_m is the minimum range, c_r is the range scaling factor, and H is the observation matrix.

r_m is the minimum range, c_r is the range scaling factor, and H is the observation matrix. \mathcal{K} is the Kalman gain. \mathcal{C} is the covariance matrix of the Kalman filter. $c(C)$ is the covariance matrix of the Kalman filter. \hat{r}_T is the estimated range of the target. z is the LiDAR measurement. T is the track. z is the LiDAR measurement.

Algorithm 2

1: **Input:**
2: $\mathcal{P}_{[k]} = \{\mathcal{P}\}$ \triangleright LiDAR trajectory k
3: $\mathcal{D}_{[k]} = \{\mathcal{D}\}$ \triangleright LiDAR detections k
4: $\mathcal{O} = \{c(v) \mid v \in \mathcal{M}, G(v) \geq G_n\}$ \triangleright obstacles k
5: $t_{[k]} \in \mathbb{R}$ \triangleright time k
6: **Persistent state:**
7: $\mathcal{T} = \{T\}$ \triangleright track $T \equiv \{\hat{x}_T, \mathbf{P}_T\}$
8: **Routine** newPointCloud($\mathcal{P}_{[k]}, \mathcal{O}$):
9: push($\mathcal{P}_{[k]}, \mathcal{B}$) \triangleright $\mathcal{P}_{[k]}$ into \mathcal{B}
10: **if** $|\mathcal{B}| > N_b$ **then**
11: pop(\mathcal{B}) \triangleright filter old
12: **end if**
13: **for** $h \in \mathcal{T}$ **do**
14: $T := \text{updateTrack}(T, \mathcal{P}_{[k]}, \mathcal{O}, t_{[k]} - t_{[k-1]})$
15: **if** $r_n(\mathbf{P}_T) > r_n$ **then**
16: $\mathcal{T} := \mathcal{T} \setminus T$ \triangleright delete
17: **end if**
18: **end for**
19: **Routine** newDetections($\mathcal{D}_{[k]}, \mathcal{O}$):
20: **for** $D \in \mathcal{D}_{[k]}$ **do**
21: $T^* := \text{initializeTrack}(D)$
22: **for** $h \in \mathcal{B}$, $t_{[i]} > t_{[k]}$ **do**
23: $T^* := \text{updateTrack}(T^*, \mathcal{P}_{[i]}, \mathcal{O}, t_{[i]} - t_{[i-1]})$
24: **end for**
25: **if** $r_n(\mathbf{P}_{T^*}) \leq r_n$ **then**
26: **if** $\forall T \in \mathcal{T}, \|\hat{r}_T - \hat{r}_{T^*}\| \leq r_n(\mathbf{P}_T) + r_n(\mathbf{P}_{T^*})$ **then**
27: $n_d(T) := n_d(T) + 1$
28: **else**
29: $\mathcal{T} := \mathcal{T} \cup T^*$
30: **end if**
31: **end if**
32: **end for**
33: **Routine** updateTrack($T, \mathcal{P}, \mathcal{O}, \Delta t$):
34: $T := \text{predictKF}(T, \Delta t)$
35: \triangleright r_n filter \hat{r}_T
36: $\mathcal{P}' := \{\mathcal{P} \mid \mathcal{P} \in \mathcal{P} \wedge \|\mathcal{P} - \hat{r}_T\| \leq r_n(\mathbf{P}_T)\}$
37: $\mathcal{K} := \text{extractClusters}(\mathcal{P}')$
38: \triangleright filter \mathcal{O}
39: $\mathcal{K}' := \{\mathcal{C} \mid \min_{c(v) \in \mathcal{O}} (\|c(\mathcal{C}) - c(v)\|) > d_m\}$
40: **if** $\mathcal{K}' \neq \emptyset$ **then**
41: \triangleright correct KF \hat{r}_T
42: $\mathcal{C}^* := \text{argmin}_{\mathcal{C} \in \mathcal{K}'} \|c(\mathcal{C}) - \hat{r}_T\|$
43: $z := c(\mathcal{C}^*)$
44: $T := \text{correctKF}(T, z)$
45: **end if**
46: **return** T

LiDAR measurement uncertainty

A. LiDAR measurement uncertainty

LiDAR measurement uncertainty \mathcal{W} . Assume the LiDAR measurement p is

$$p = l_{gt} \mathbf{R}_{gt} \vec{d} + t_{gt}. \quad (34)$$

LiDAR measurement \mathcal{W} , l_{gt} is the LiDAR range \vec{d} is the LiDAR direction

A LiDAR measurement w is defined as

$$w = [t_n \quad \alpha_n \quad \beta_n \quad \gamma_n \quad l_n]^\top, \quad (35)$$

$$w \sim \mathcal{N}(\mathbf{0}, \Sigma_w), \quad (36)$$

LiDAR measurement Σ_w is defined as

$$t_m = t_{gt} + t_n, \quad (37)$$

$$\mathbf{R}_m = \mathbf{R}_{zm} \mathbf{R}_{ym} \mathbf{R}_{xm} \quad (38)$$

$$= \mathbf{R}_z(\gamma_{gt} + \gamma_n) \mathbf{R}_y(\beta_{gt} + \beta_n) \mathbf{R}_x(\alpha_{gt} + \alpha_n), \quad (39)$$

$$l_m = l_{gt} + l_n.$$

Non-holonomic odometry

LiDAR measurement \mathbf{R}_{gt} is defined as

LiDAR measurement x, y, z is defined as

LiDAR measurement p_m is defined as

LiDAR measurement l_m is defined as (34):

$$p_m = P_m(w) = l_m \mathbf{R}_m \vec{d} + t_m. \quad (40)$$

LiDAR measurement P_m is defined as

LiDAR measurement Σ_w is defined as

$$\Sigma = \mathbf{J} \Sigma_w \mathbf{J}^\top, \quad \mathbf{J} = \frac{\partial P_m(w)}{\partial w}, \quad (41)$$

LiDAR measurement \mathbf{J} is defined as

$$\mathbf{J} = \begin{bmatrix} \mathbf{I} & l_m \mathbf{R}_{zy} \frac{\partial \mathbf{R}_x}{\partial \alpha_n} \vec{d} & l_m \mathbf{R}_{zm} \frac{\partial \mathbf{R}_y}{\partial \beta_n} \mathbf{R}_{xm} \vec{d} & l_m \frac{\partial \mathbf{R}_z}{\partial \gamma_n} \mathbf{R}_{yx} \vec{d} & \mathbf{R}_m \vec{d} \end{bmatrix}, \quad (42)$$

LiDAR measurement $\mathbf{R}_{zy} = \mathbf{R}_{zm} \mathbf{R}_{ym}$ and $\mathbf{R}_{yx} = \mathbf{R}_{ym} \mathbf{R}_{xm}$. Then μ is defined as

$$\mu = \mathbb{E}[P_m(w)] = P_m(w = \mathbf{0}) = p_m. \quad (43)$$

LiDAR measurement P_m is defined as

$$f_{P_m}(p) \approx f_{\mathcal{N}}(p, \mu, \Sigma), \quad (44)$$

LiDAR measurement μ is defined as

$$\Sigma.$$

B. Evaluation of voxel hit probability

LiDAR measurement p_m is defined as

$$p_m, \text{ is defined as}$$

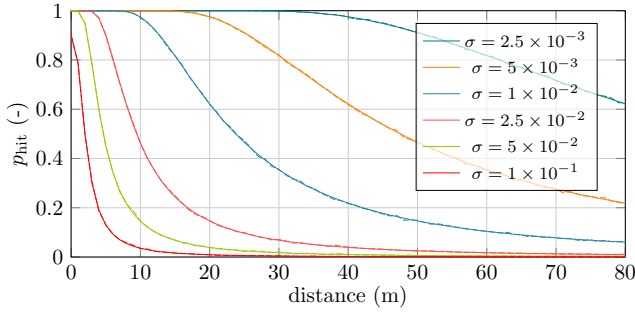


Fig. 5: Probability of hit by LiDAR sensor as a function of distance and σ .

$$p_h = p(v_m = v_{gt}) = p(\mathbf{p} \in v_m | \mathbf{p}_m, \Sigma), \quad (45)$$

$$v_m = v(\mathbf{p}_m) \quad v_{gt} = v(\mathbf{p}).$$

$$p_h = \int_{v_m} f_{\mathcal{N}}(\mathbf{x}, \boldsymbol{\mu}, \Sigma) d\mathbf{x}, \quad (46)$$

$$f_{\mathcal{N}}(\mathbf{x}, \boldsymbol{\mu}, \Sigma)$$

C. Target detection probability over distance

If we consider the probability of hit by LiDAR sensor as a function of distance and σ , we can write the probability of hit by LiDAR sensor as a function of distance and σ .

$$r \in S, \quad f_r(r) = \frac{1}{A_S} = \frac{1}{4\pi l^2}, \quad (47)$$

$$f_r(r) = \frac{1}{A_S} = \frac{1}{4\pi l^2}, \quad (47)$$

$$f_r(r) = \frac{1}{A_S} = \frac{1}{4\pi l^2}, \quad (47)$$

$$f_r(r) = \frac{1}{A_S} = \frac{1}{4\pi l^2}, \quad (47)$$

$$f_r(r) = \frac{1}{A_S} = \frac{1}{4\pi l^2}, \quad (47)$$

$$f_r(r) = \frac{1}{A_S} = \frac{1}{4\pi l^2}, \quad (47)$$

$$p_{h,r} = p(r \in P'_r) = \int_{P'_r} f_r(r) dr = \frac{A_{P'_r}}{A_S} = \frac{A_{P_r}}{4\pi l^2}, \quad (48)$$

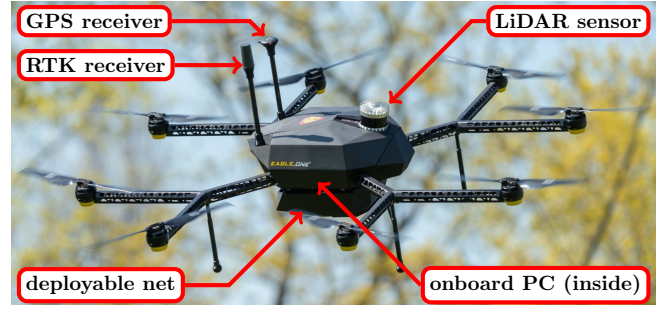


Fig. 6: A photograph of the M4 UAV used in the experiments.

model	horiz. rays	vertical rays	vertical FOV	scan rate	max. range	precision
OS0-128	1024	128	$\pm 45^\circ$	10 Hz	50 m	± 5 cm
OS1-128	1024	128	$\pm 22.5^\circ$	10 Hz	100 m	± 5 cm

Tab. 1: Parameters of the LiDAR sensors used in the experiments.

$$A_{P'_r} = A_{P_r} \quad P'_r \in \mathcal{R} \quad (49)$$

$$P'_r = \{r \in S | \exists P'_r, r \in P'_r\} \quad P'_r \in \mathcal{R}$$

See (49) for details.

$$A_{P_r} \equiv A_{P_r} \quad r \in \mathcal{R}$$

V. EXPERIMENTAL EVALUATION

To evaluate the performance of the proposed method, we conducted experiments using a M4 UAV equipped with a LiDAR sensor, RTK-GPS, a IMU, and a deployable net.

The LiDAR sensor used in the experiments is the OS0-128 (see Tab. 1). The UAV used in the experiments is the M4 UAV (see Fig. 6). The UAV is equipped with a LiDAR sensor, RTK-GPS, a IMU, and a deployable net. The UAV is equipped with a LiDAR sensor, RTK-GPS, a IMU, and a deployable net.

A. Simulated experiments

To evaluate the performance of the proposed method, we conducted simulated experiments using a LiDAR sensor, RTK-GPS, a IMU, and a deployable net. The LiDAR sensor used in the experiments is the OS0-128 (see Tab. 1).

occupancy mapping						
v_s	g_o	g_h	g_e	G_b	G_n	G_a
0.25 m	0	-740	-1000	-0.1	-300	-750
clustering, raycasting and separate voxel removal						
d_b	d_h	d_n	d_m	n_b	n_m	n_a
0.25 m	0.7 m	3 m	20 m	24		
multi-target tracking						
N_b	c_r	r_m	r_n	n_b	n_m	Z
10	0.5	1.5 m	3 m	24		1 m
Ξ_r	Ξ_v	Ξ_a	$P_{0,r}$	$P_{0,v}$	$P_{0,a}$	
0.5 m	0.5 ms ⁻¹	0.1 ms ⁻²	0.5 m	3 ms ⁻¹	3 ms ⁻²	

Table III: Parameters (see III).

Algorithm 1

Algorithm 2

Algorithm 3

Algorithm 4

Algorithm 5

Algorithm 6

Algorithm 7

Algorithm 8

Algorithm 9

Algorithm 10

Algorithm 11

Algorithm 12

Algorithm 13

Algorithm 14

Algorithm 15

Algorithm 16

Algorithm 17

Algorithm 18

Algorithm 19

Algorithm 20

Algorithm 21

Algorithm 22

Algorithm 23

Algorithm 24

Algorithm 25

Algorithm 26

Algorithm 27

Algorithm 28

Algorithm 29

Algorithm 30

Algorithm 31

Algorithm 32

Algorithm 33

Algorithm 34

Algorithm 35

Algorithm 36

Algorithm 37

Algorithm 38

Algorithm 39

Algorithm 40

Algorithm 41

Algorithm 42

Algorithm 43

Algorithm 44

Algorithm 45

Algorithm 46

Algorithm 47

Algorithm 48

Algorithm 49

Algorithm 50

Algorithm 51

Algorithm 52

Algorithm 53

Algorithm 54

Algorithm 55

	mean position error	std. dev. of pos. error
simulation	0.17 m (0.24 m)	0.10 m (0.24 m)
real-world	0.92 m (0.91 m)	0.98 m (0.76 m)

Table III: Results (in m).

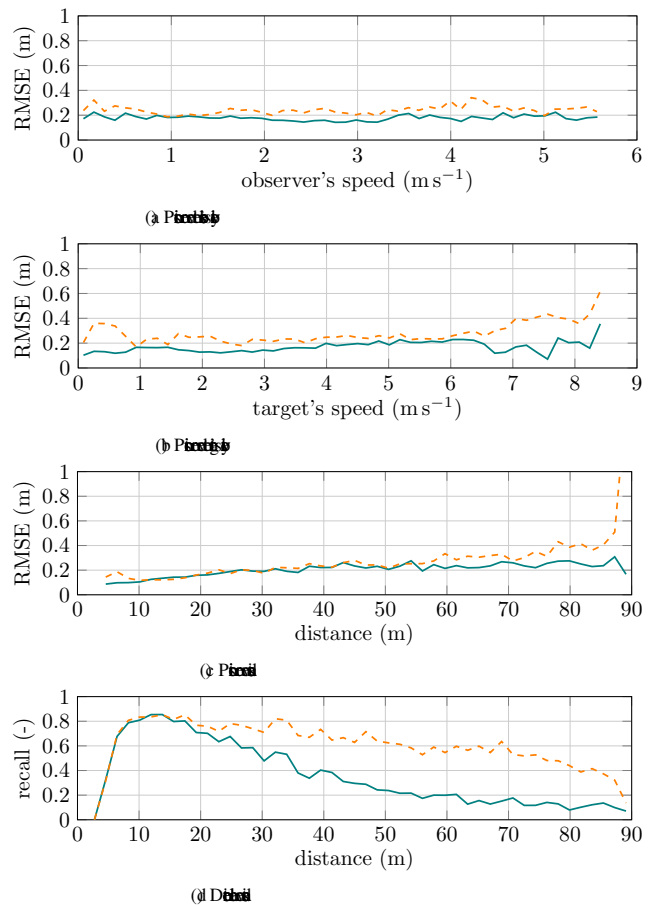


Fig. 7: Results (in m).

Algorithm 1

Algorithm 2

Algorithm 3

Algorithm 4

Algorithm 5

Algorithm 6

REFERENCES

- [1] V. Ch. P. K. A. A. N. N. G. d. M. G. A. *Ad Hoc Networks*, **111**, p 102324, 2021. DOI: 10.1016/j.adhoc.2021.102324
- [2] F.-L. C. A. M. C. V. I. M. R. C. d. O. F. *Sensors*, **22**, **4**, 2022. DOI: 10.3390/s22041453
- [3] M. G. d. M. M. F. *Safety Science*, **139**, p 105273, 2021. DOI: 10.1016/j.ssci.2021.105273
- [4] M. S. A. S. U. J. H. J. T. C. W. d. C. R. *Journal of Intelligent & Robotic Systems*, **103**, **1**, p 145, 2021.

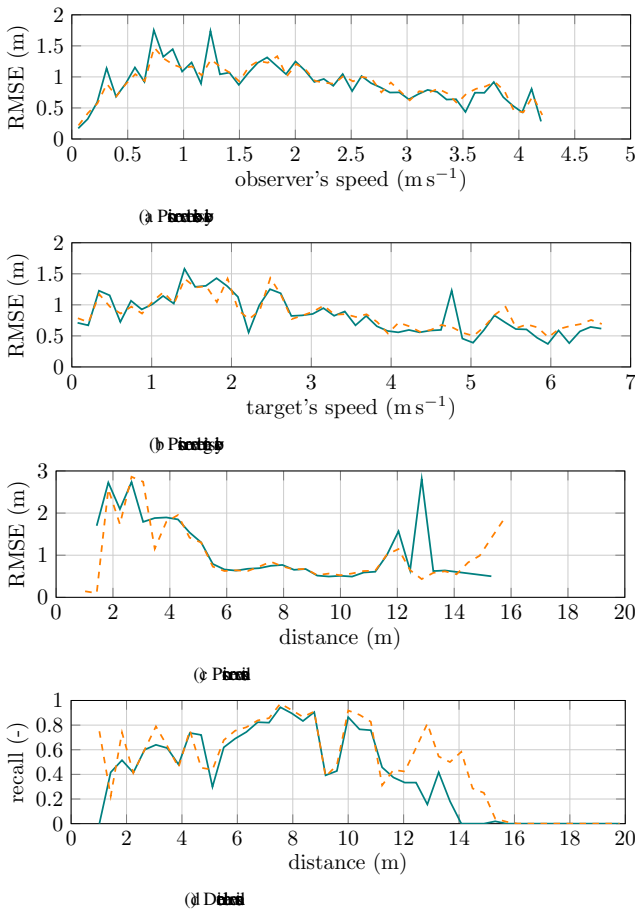


Fig: Results of the proposed method

[5] M. V. D. He *et al.*, *RA-L*, **4**, **4**, p34023409, Oct 2019.

[6] M. V. M. S. *et al.*, *RA-L*, **5**, **2**, p24592466, Apr 2020.

[7] M. G. *et al.*, *ICUAS*, 2020, p3240.

[8] M. B. S. B. *et al.*, *SSRR*, 2020, p3441.

[9] M. K. T. A. F. S. H. T. M. K. T. N. K. I. N. K. *et al.*, *Journal of Field Robotics*, **38**, **7**, p933966, 2021.

[10] A. B. *et al.*, *Field Robotics*, **2**, **1**, p222240, 2022.

[11] M. V. Y. S. T. B. *et al.*, *Robotics and Autonomous Systems*, **149**, p103970, Mar 2022.

[12] V. P. M. V. P. S. P. M. S. C. *et al.*, *2022 International Conference on Unmanned Aircraft Systems (ICUAS)*, IEEE, Jul 2022, p526535.

[13] J. P. S. P. K. D. K. M. S. P. K. *et al.*, *T-MTT*, **67**, **3**, p12214232, 2019.

[4] A. D. Q. F. I. U. J. G. M. A. A. L. P. D. *et al.*, *IRS*, 2018, p140.

[5] Z. S. X. C. C. Z. W. D. J. W. A. *et al.*, *TVT*, **69**, **3**, p27312739, 2020.

[6] F. S. C. E. F. A. F. R. T. D. D. *et al.*, *arXiv e-prints*, p2007.07396, Jul 2020.

[7] M. H. B. B. M. H. B. M. A. S. U. A. V. *et al.*, *Laser Radar Technology and Applications XXIV*, M. D. T. G. W. K. E. S. *et al.*, SPIE, 2019, p99-108.

[8] S. D. L. M. Q. D. *et al.*, *IEEE Robotics and Automation Letters*, **7**, **2**, p30623069, 2022.

[9] A. B. *et al.*, *IEEE Robotics and Automation Letters*, **7**, **2**, p37573764, 2022.

[20] A. S. L. S. K. T. S. H. B. *et al.*, *AVSS*, Aug 2017, p16.

[21] A. R. V. L. P. F. *et al.*, *IEEE Transactions on Pattern Analysis and Machine Intelligence*, **39**, **5**, p879892, 2017.

[22] A. C. J. T. S. V. P. S. P. C. *et al.*, *Access*, **8**, p3048030490, 2020.

[23] M. P. P. P. V. K. T. M. Y. S. M. V. B. T. B. D. H. M. P. K. T. S. H. M. S. *et al.*, *preprint arXiv:2206.08185*, 2022.

[24] J. S. S. L. O. A. M. *et al.*, *Robotics: Science and Systems*, **2**, **9**, 2014.

[25] A. H. K. M. W. M. B. C. S. W. B. *et al.*, *Autonomous robots*, **34**, **3**, p189206, 2013.

[26] D. M. G. *et al.*, *Computer graphics and image processing*, **19**, **2**, p129447, 1982.

[27] D. D. P. J. S. U. A. *et al.*, *IEEE Robotics and Automation Letters*, **5**, **4**, p64116418, 2020.

[28] D. D. G. L. D. S. S. *et al.*, *2017 IEEE International Conference on Robotics and Automation (ICRA)*, 2017, p25692576.

[29] R. B. R. S. C. 3D *et al.*, *IEEE International Conference on Robotics and Automation (ICRA)*, Sep 2011, p13-2011.

[30] G. G. B. J. *et al.*, *2010*.

[31] M. Q. K. C. B. P. G. J. F. T. F. J. L. B. R. W. *et al.*, *ICRA Workshop on Open Source Software*, 2009.

[32] T. B. M. P. K. M. V. B. V. S. P. R. P. H. D. H. *et al.*, *Journal of Intelligent & Robotic Systems*, **102**, **26**, p128, May 2021.

[33] H. M. A. E. *et al.*, *Proceedings. 1985 IEEE International Conference on Robotics and Automation*, **2**, 1985, p116421.

[34] C. O' M. H. W. T. D. N. M. H. *et al.*, *IEEE Robotics and Automation Letters*, **4**, **2**, p20152022, 2019.

[35] P. P. V. K. M. P. K. T. B. A. R. K. M. S. *et al.*, *IEEE Robotics and Automation Letters*, **6**, **4**, p75967603, Oct 2021.

[36] V. K. K. Y. P. P. E. *et al.*, *Journal of Field Robotics*, **38**, **8**, p10364058, May 2021.

[37] Y. X. Y. T. G. R. Y. G. O. H. S. H. *et al.*, *Robotics and Autonomous Systems*, **134**, p103649, 2020.

- [8] R. B. Russett, "A new method for the automatic detection of aircraft in radar returns," *IEEE Transactions on Aerospace and Electronic Systems*, vol. 1, no. 1, pp. 1-10, 1965.
- [9] J. A. Woerner, et al., "A new method for the automatic detection of aircraft in radar returns," *Eurographics*, vol. 87, no. 3, 1987, p.340.
- [10] A. G. N. N. N., "A new method for the automatic detection of aircraft in radar returns," *Statistics and Computing*, vol. 14, pp. 251-260, 2004.
- [11] D. H. T. Ba P. K. V. S. M. P. M. V. D. K. P. S. V. W. P. S. J. H. V. P. G. S. D. B. L. P. S. R. P. T. N. M. S. MRS MUAV H. P. S. R. R. W. D. C. E. n. 2022 International Conference on Unmanned Aircraft Systems (ICUAS). IEEE, Jan 2022, p.1264-273.